

# EE-MLLM: A Data-Efficient and Compute-Efficient Multimodal Large Language Model

Feipeng Ma<sup>1,2\*</sup> Yizhou Zhou<sup>2</sup> Hebei Li<sup>1</sup> Zilong He<sup>1</sup> Siying Wu<sup>3</sup>  
Fengyun Rao<sup>2</sup> Yueyi Zhang<sup>1</sup> Xiaoyan Sun<sup>1,3†</sup>

<sup>1</sup>University of Science and Technology of China <sup>2</sup>WeChat, Tencent Inc.

<sup>3</sup>Institute of Artificial Intelligence, Hefei Comprehensive National Science Center  
maf@ustc.edu.cn harryizhou@tencent.com {zhyuey,sunxiaoyan}@ustc.edu.cn

## Abstract

In the realm of multimodal research, numerous studies leverage substantial image-text pairs to conduct modal alignment learning, transforming Large Language Models (LLMs) into Multimodal LLMs and excelling in a variety of visual-language tasks. The prevailing methodologies primarily fall into two categories: self-attention-based and cross-attention-based methods. While self-attention-based methods offer superior data efficiency due to their simple MLP architecture, they often suffer from lower computational efficiency due to concatenating visual and textual tokens as input for LLM. Conversely, cross-attention-based methods, although less data-efficient due to additional learnable parameters, exhibit higher computational efficiency by avoiding long sequence input for LLM. To address these trade-offs, we introduce the Data-Efficient and Compute-Efficient Multimodal Large Language Model (EE-MLLM). Without introducing additional modules or learnable parameters, EE-MLLM achieves both data and compute efficiency. Specifically, we modify the original self-attention mechanism in MLLM to a composite attention mechanism. This mechanism has two key characteristics: 1) Eliminating the computational overhead of self-attention within visual tokens to achieve compute efficiency, and 2) Reusing the weights on each layer of LLM to facilitate effective modality alignment between vision and language for data efficiency. Experimental results demonstrate the effectiveness of EE-MLLM across a range of benchmarks, including general-purpose datasets like MM-Bench and SeedBench, as well as fine-grained tasks such as TextVQA and DocVQA.

## Introduction

Recently, Large Language Models (LLMs) have gained significant attention due to their surprising performance on various natural language tasks. However, real-world scenarios often involve more than just linguistic modality, making it crucial to extend LLM to Multimodal LLMs. The key to expansion is to perform modality alignment, that is, to learn to map the remaining modalities with the same semantics to their corresponding language modality in the feature space of the pre-trained LLM.

\*This work was performed during Feipeng Ma’s internship at WeChat, Tencent Inc.

†Corresponding author

In the field of multimodal LLM research involving vision and language, a series of research works on modality alignment have been carried out and achieved excellent performance. These methods can be roughly divided into two categories: self-attention-based methods and cross-attention-based methods.

The self-attention-based methods firstly leverage a simple MLP layer to project the visual tokens into the input space of LLM, and then concatenate the visual tokens with the textual tokens, which is shown in Fig.1 (1). These flattened concatenated long token sequences are fed into the LLM to further model the dependencies of various tokens. These methods exhibit great data efficiency due to two factors: 1) The alignment module is simple and has a small number of learnable parameters. 2) Visual tokens aligned in the input space of LLM will naturally lead to the alignment between vision and language in each layer of LLM. Therefore, the training procedure does not need to focus on the modality alignment within the LLM, enabling data efficiency. For example, LLaVA (Liu et al. 2023b) achieves promising performance by pre-training on only 558k data and fine-tuning on only 665k instruction data. However, the flattening operation of directly concatenating visual tokens and textual tokens expands the length of the token sequence from  $T$  to  $V + T$  (where  $T$  is the number of textual tokens,  $V$  is the number of visual tokens), and the computational cost of the language model layer (self-attention structure) increases from  $O(T^2)$  to  $O((V + T)^2)$ , results in lower computer-efficiency. Especially when the input image is high-resolution, the number of visual tokens increases, and the compute inefficiency will prolong the training and inference time. Specifically, LLaVA (Liu et al. 2023b) and Deepseek-VL (Lu et al. 2024) have 576 visual tokens, Sphinx (Lin et al. 2023) utilizes 2,890 visual tokens.

The cross-attention-based methods directly insert new cross-attention layers between existing pre-trained language model layers. As shown in Fig.1 (2), the keys and values in these layers are obtained from the visual tokens while the queries are derived from the text tokens. These methods have higher compute efficiency because the length of the input sequence is always kept as  $T$  and does not increase with the increase of visual tokens. However, these methods usually require a large amount of pre-training data, leading to data inefficiency. For example, Flamingo (Alayrac et al. 2022)

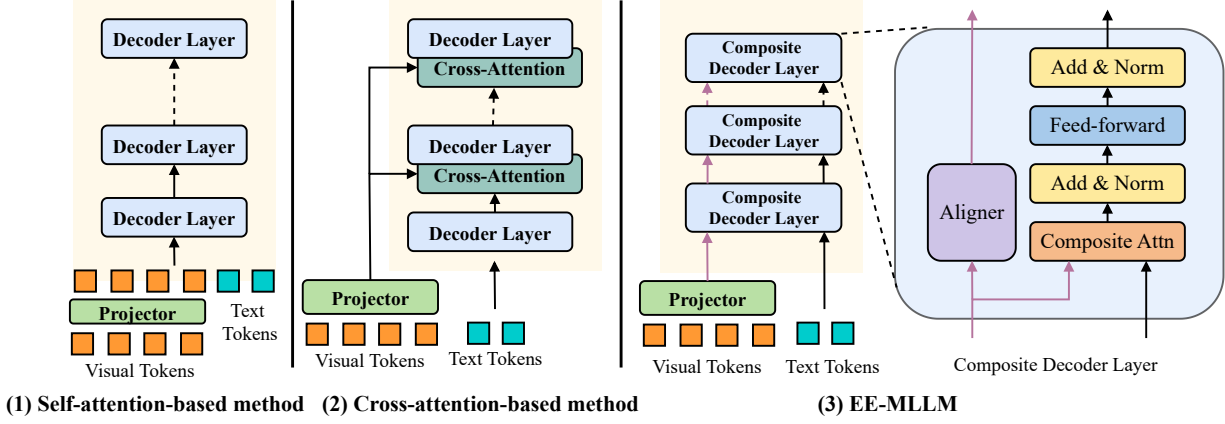


Figure 1: Architecture comparisons between self-attention-based method, cross-attention-based method and our EE-MLLM. (1) The self-attention-based mechanism utilizes a projector to align visual tokens with text tokens, subsequently concatenating these tokens as input for the LLM. (2) The cross-attention-based mechanism integrates additional cross-attention blocks into the decoder layers. (3) EE-MLLM introduces a composite attention mechanism to eliminate the computational overhead of self-attention within visual tokens and reuse the weights as aligners on each layer of LLM to facilitate modality alignment.

is pre-trained on 1.8 billion image-text pairs (Jia et al. 2021) and interleaved data. EVLM (Chen et al. 2024) is pre-trained on 2.5 billion image-text pairs and 50 million interleaved image-text data. This data inefficiency arises from two factors: 1) The additional cross-attention layers will introduce a large number of learnable parameters, necessitating more training data. 2) The training procedure has to focus on the modality alignment between vision and language on different layers of LLM, posing a huge optimization complexity for modality alignment.

By reviewing existing methods, we conclude that the key points to ensure data efficiency and compute efficiency are 1) Avoiding an increase in the length of input sequence for LLM, 2) The modality alignment module should have fewer parameters, and the alignment needs to be effective. Taking two summary viewpoints into account, we present a data-Efficient and compute-Efficient Multimodal Large Language Model (EE-MLLM). Specifically, we propose a composite attention mechanism to replace the original self-attention mechanism in MLLM. The composite attention mechanism has two features: 1) Eliminating the computational overhead of self-attention within visual tokens to achieve compute efficiency. The original self-attention mechanism of MLLM consists of three components: self-attention within visual tokens, self-attention within text tokens, and cross-attention between text and visual tokens. We observe that the self-attention within visual tokens is redundant. This is because a) the interaction between visual tokens is already well-processed by the vision encoder, and b) LLM can facilitate the implicit interaction among visual tokens via the information aggregation property of LLM (Wang et al. 2023b). Therefore, we eliminate the self-attention within visual tokens and maintain the length of the input sequence for LLM as the length of text tokens, thereby facilitating computational efficiency. 2) Instead of introducing additional modules like cross-attention-based methods,

we reuse the weights on each layer of LLM to facilitate effective modality alignment between vision and language for data efficiency. As a result, without introducing additional parameters, visual tokens aligned in the input space of LLM can naturally facilitate the alignment between vision and language in each layer of LLM. This means the training procedure does not need to focus on the modality alignment within the LLM, which enables data efficiency.

To demonstrate the effectiveness of EE-MLLM, we evaluate its performance on both general benchmarks and fine-grained benchmarks, such as MMBench-EN, MME, ScienceQA, AI2D, TextVQA, and DocVQA. In comparison with state-of-the-art MLLMs, our EE-MLLM exhibits promising results on both general and fine-grained benchmarks. Simultaneously, EE-MLLM proves to be computationally efficient in the inference stage. When applied to high-resolution image inputs, EE-MLLM maintains comparable performance at a significantly reduced computational cost. For instance, with a  $980 \times 980$  input image, the number of visual tokens can reach 4,900, and the FLOPs of EE-MLLM are 70% of those in self-attention-based methods. We also assess the inference speed of EE-MLLM in a real-world scenario, confirming its efficiency. Specifically, when the number of generated tokens is set to 32, EE-MLLM achieves an inference speed of 77 tokens per second on a single NVIDIA H800 GPU, which is 1.9 times faster than self-attention-based methods at the same resolution  $980 \times 980$ . Our main contributions are summarized as follows:

1. We revisit modality alignment in multimodal LLMs, pointing out the issue of efficiency and efficacy in self-attention-based and cross-attention-based methods.
2. We propose a composite attention mechanism for EE-MLLM to enhance the data and computational efficiency.
3. Our EE-MLLM achieves outstanding performance on a variety of benchmarks, while the inference speed is much improved.

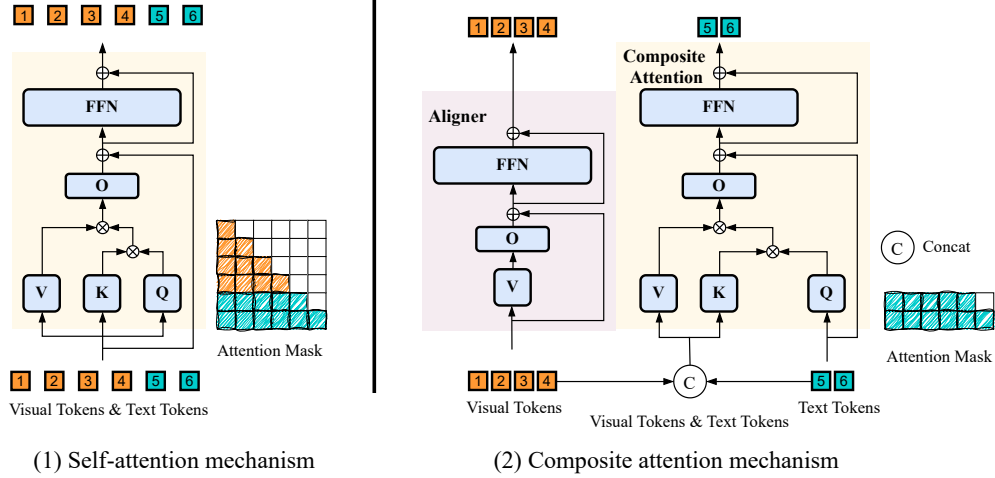


Figure 2: Our composite attention mechanism consists of the composite attention module and the aligner. For the aligner, visual tokens are aligned to the feature space of each layer of LLM by the aligner alone; for the composite attention module, the concatenation of visual and text tokens are used as keys and values, and the text tokens are used as queries for attention, thus eliminating the self-attention within visual tokens.

## Related Work

**Self-attention-based methods.** Self-attention-based methods (Dai et al. 2024; Zhu et al. 2024; Chen et al. 2023a; Bai et al. 2023; Chen et al. 2023b; Fang et al. 2023) employ a projector to align visual features with the input space of LLM. LLaVA (Liu et al. 2023b,a) uses a simple MLP layer to connect the vision encoder of CLIP (Radford et al. 2021) with Vicuna (Zheng et al. 2023). DeepSeek-VL (Lu et al. 2024) employs hybrid vision encoders, including SigLIP (Zhai et al. 2023) for high-level semantic features and SAM-B (Kirillov et al. 2023) for low-level features. Considering the scenarios that require fine-grained information, such as document recognition and form understanding, recent work extends MLLM to support high-resolution inputs. LLaVA-Next (Liu et al. 2024) proposes dividing the image into small patches for extracting local features and concatenating the downsampled image feature as global context. Monkey (Li et al. 2024b) also partitions high-resolution images into small patches, processing each patch independently with a trainable resampler. Since the self-attention-based methods are compute-inefficient, the overhead for high-resolution inputs can be more severe. Deco (Yao et al. 2024) and HoneyBee (Cha et al. 2024) carefully design projectors to reduce the number of visual tokens with minimal information loss. However, these methods still compromise fine-grained capabilities when reducing the number of visual tokens. Our EE-MLLM, a cross-attention-based architecture, achieves state-of-the-art performance while maintaining computational efficiency.

**Cross-attention-based methods.** Cross-attention-based methods (Laurençon et al. 2023; Alayrac et al. 2022; Awadalla et al. 2023; Chen et al. 2024) typically incorporate additional cross-attention modules into the decoder layers of LLM to integrate visual information without extending

the length of the text token sequence. Flamingo (Alayrac et al. 2022) introduces a novel gated xattn-dense block, incorporating a tanh-gating mechanism for training stability. Flamingo is trained on large-scale interleaved image-text data and supports in-context few-shot learning. EVLM (Chen et al. 2024) enhances Flamingo by: (1) utilizing hierarchical ViT features without a resampler, (2) replacing the image token with a set of learnable tokens in the text input, and (3) introducing MoE to boost performance. Although these cross-attention-based methods are computationally efficient, the additional cross-attention blocks lead to a large number of trainable parameters and a heavy reliance on pre-training data. Our EE-MLLM avoids introducing any extra trainable parameters and repurposes the weights of LLM to map visual tokens into the LLM feature space, thus achieving promising performance with a small amount of training data.

## Method

### Model Architecture

EE-MLLM comprises a visual encoder, a two-layer MLP serving as the projector, and the LLM with composite decoder layers. We propose a composite attention mechanism and design a composite decoder layer for EE-MLLM to achieve data efficiency and compute efficiency. The composite decoder layer consists of an aligner and a composite attention module.

**Composite Attention Module.** The original self-attention mechanism comprises self-attention within visual tokens, self-attention within text tokens, and cross-attention between text tokens and visual tokens. We observe that self-attention within visual tokens is redundant for two reasons: 1) The interaction between visual tokens is already well-learned in the vision encoder, and 2) LLM can enable the

Type	Dataset	Ratio
General Instruction Data	ShareGPT4V	35%
	LVIS-Instruct4V	
	LAION-GPT4V	
	TextOCR-GPT4V	
	Localized Narratives	
Text-Centric Data	IconQA	8.5%
	DVQA	
	PlotQA	
	CLEVR	
	DocVQA	
	ChartQA	
Others	ScienceQA	47%
	Text-only data	
	In-house data	9.5%

Table 1: Details of supervised fine-tuning data.

implicit interaction between visual tokens via the information aggregation property (Wang et al. 2023b). Therefore, we eliminate self-attention within visual tokens and obtain the composite attention module. We assume that visual tokens  $I \in \mathbb{R}^{k \times h}$  and text tokens  $T \in \mathbb{R}^{n \times h}$ , where  $k$  and  $n$  are the lengths of visual tokens and text tokens, respectively. And  $h$  denotes the dimension of hidden states. The original self-attention can be formulated as follows:

$$\text{Attention}(X^q, X^k, X^v) = \text{softmax}\left(\frac{X^q X^k T}{\sqrt{h}}\right) X^v, \quad (1)$$

where  $X^q = [I; T]W_q$ ,  $X^k = [I; T]W_k$ ,  $X^v = [I; T]W_v$ ,  $W_q$ ,  $W_k$  and  $W_v$  are the weights of the self-attention module. The symbol  $[:]$  denotes the concatenation operation of two variables in the sequence dimension. As illustrated in Fig. 2, our composite attention module uses text tokens as the queries and the concatenation of visual tokens and text tokens as keys and values for cross-attention. Specifically,  $X^q = TW_q$ ,  $X^k = [I; T]W_k$ , and  $X^v = [I; T]W_v$ . The length of the output sequence will be  $n$ , which is the same as the length of text tokens  $T$ . The attention mask for self-attention is a lower triangular matrix, whereas the attention mask for the composite attention module is a trapezoidal matrix. This implies that text tokens will attend to all previous tokens, including visual tokens, while the interaction within visual tokens is eliminated.

**Aligner.** We introduce the aligner, which leverages the existing weights at each layer of LLM to enhance modality alignment between vision and language without the need for additional modules such as cross-attention-based methods. By reusing these weights, visual tokens aligned in the input space of the LLM can naturally facilitate modality alignment at each layer. This approach eliminates the necessity for the training procedure to concentrate on modality alignment within the LLM, thereby promoting data efficiency. As depicted in Fig. 2, in each layer, text tokens are mapped by the value matrix ( $W_v$ ), output matrix ( $W_o$ ), and FFN. Hence, we make visual tokens follow the same mapping relationship in the aligner. Specifically, the aligner comprises  $W_v$ ,  $W_o$ , and FFN, which share weights with the corresponding LLM modules. The residual connection is also implemented

in the aligner. The aligner can be formulated as follows:

$$H = IW_v W_o + I \quad (2)$$

$$O = \text{FFN}(H) + H. \quad (3)$$

This can be viewed as a decoder block without attention.

## Analysis of the Computational Overhead

Our EE-MLLM can reduce the computational overhead without introducing additional parameters. In this section, we analyze the compute efficiency of EE-MLLM from the perspective of FLOPs, comparing it with LLaVA. The LLM consists of  $d$  blocks, with a hidden states dimension of  $h$ , an input text length of  $T$ , and  $V$  visual tokens. Considering an LLM, we assume the input sequence length is  $L$ , the FLOPs of the self-attention module and FFN are  $8Lh^2 + 4L^2h$  and  $16Lh^2$ . For self-attention-based methods, such as LLaVA, the length of the input sequence is  $L = V + T$ . Therefore, the FLOPs of LLaVA are  $24(T + V)dh^2 + 4(T + V)^2dh$ . For EE-MLLM, the FLOPs of composite attention modules are  $(6T + 2V)h^2 + 4VTdh + 4T^2h$ . Given that we introduce aligners, the FLOPs of FFN are the same as those of LLaVA, which are  $16(V + T)h^2$ . The aligners introduce an additional matrix multiplication by  $O$ , adding  $2Vh^2$  FLOPs. Therefore, the total FLOPs of EE-MLLM are  $2(11T + 10V)dh^2 + 4VTdh + 4T^2dh$ . Particularly, when the resolution of the input image is  $980 \times 980$ , the number of visual tokens is 4,900, and the length of text tokens is 256, which is a typical length during training, the FLOPs of EE-MLLM amount to 70% of those of LLaVA.

## Experiments

### Implementation Details

**Model Configurations.** We employ Vicuna-7b-v1.5 (Zheng et al. 2023) as our LLM and SigLIP (Zhai et al. 2023) as the vision encoder. Specifically, SigLIP is initialized from Idefics2 (Laurençon et al. 2024), which supports dynamic resolutions up to  $980 \times 980$ . The projector consists of a two-layer MLP, identical to that of LLaVA (Liu et al. 2023b).

**Pre-training Configurations.** During the pre-training stage, we follow LLaVA to adopt blip-558k (Li et al. 2022) for training one epoch. We freeze the LLM and the vision encoder, making only the projector trainable. We adopt AdamW (Loshchilov and Hutter 2018) optimizer. The learning rate is  $1e-3$ , followed by a linear warm-up scheduler and then a cosine decay scheduler. The global batch size is 256.

**Fine-tuning Configurations.** During the fine-tuning stage, we freeze the vision encoder and update the weights of LLM and projector. The total quantity of supervised fine-tuning data amounts to 3 million. As displayed in Tab. 1, following Deepseek-VL (Lu et al. 2024), our supervised fine-tuning data incorporates open-source gpt4v datasets, including ShareGPT4V (Chen et al. 2023b), LVIS-Instruct4V (Wang et al. 2023a), LAION-GPT4V (LAION 2023), and TextOCR-GPT4V (Carter 2024). Moreover, to enhance the fine-grained capabilities of MLLM, we introduce DVQA (Kafle et al. 2018), PlotQA (Methani et al. 2020), CLEVR (Johnson et al. 2017), DocVQA (Mathew, Karatzas, and Jawahar 2021), ChartQA (Masry et al. 2022),

Model	LLM	MMB-T	MME	ScienceQA	HallB	MMMU	CCBench	SeedBench	BLINK
InstructBLIP	Vicuna-7B	36.0	1137.1	54.7	31.2	30.6	12.7	44.5	-
MiniGPT-4-v1	Vicuna-7B	12.2	770.6	39.0	31.9	23.6	1.8	31.6	-
MiniGPT-4-v2	Llama2-7B	24.3	708.4	54.1	30.0	25.0	1.4	29.4	-
Idefics-instruct	Llama-7B	48.2	942	51.6	27.3	18.4	7.8	45.0	38.3
OpenFlamingo v2	MPT-7B	6.6	535	45.7	29.4	28.2	6.3	28.8	-
Qwen-VL	Qwen-7B	38.2	334.1	57.7	29.9	29.6	6.1	52.5	27.9
Qwen-VL-Chat	Qwen-7B	60.6	1467.8	65.5	36.8	37.0	41.2	64.8	28.2
VLoRA	Vicuna-7B	63.4	1311.3	66.4	26.4	36.0	28.6	-	-
ShareGPT4V	Vicuna-7B	64.6	1561.4	68.2	28.6	37.2	30.8	69.3	40.9
LLaVA-v1.5	Vicuna-7B	62.3	1510.7	66.8	27.6	35.7	27.5	65.8	39.7
LLaVA-v1.6	Vicuna-7B	66.5	1475.6	68.5	27.6	37.6	24.3	69.6	41.6
EE-MLLM	Vicuna-7B	70.4	1528.1	77.7	38.6	33.4	37.3	70.2	43.2

Table 2: Comparison with state-of-the-art methods on general benchmarks, including MMBench, MME, ScienceQA, HallusionBench, MMMU, CCBench, SeedBench, and BLINK. MMB-T indicates we report the results on MMBench-TEST-EN-V11.

and ScienceQA (Lu et al. 2022) for fine-tuning. To preserve language abilities during fine-tuning, we utilize a large volume of text-only data from various sources. The text-only data encompasses various dataset types, such as mathematical reasoning, multi-round dialogues, logic comprehension, and code. Meanwhile, the in-house data primarily consists of OCR-related, table and diagram comprehension, and mathematical reasoning data. The optimizer is AdamW with a global batch size of 128. The learning rate is  $2e-5$  and the learning rate scheduler is the same as the pre-training stage. The training is conducted on 16 NVIDIA H800 GPUs.

## Evaluation Benchmarks

We conduct our evaluations using the VLMEvalKit (Duan et al. 2024), and the results of other state-of-the-art models are obtained from the same source.

**General Benchmarks.** 1) MMBench-EN (Liu et al. 2023c) is a comprehensive multimodal benchmark specifically designed to assess the performance of MLLMs. It comprises over 3,000 multiple-choice questions spanning 20 ability categories. We evaluate EE-MLLM on the MMBench-EN-V1.1. 2) MME (Fu et al. 2023) evaluates advanced MLLMs in terms of perception and cognition, encompassing a total of 14 subtasks. To minimize the impact of prompt engineering on MLLMs, MME’s instructions are designed to elicit simple binary responses, such as “please answer yes or no.”. We report the results of the perception split of MME. 3) ScienceQA (Lu et al. 2022) is derived from elementary and high school science curricula. The questions in ScienceQA cover three subjects: natural science, language science, and social science. 4) HallusionBench (Guan et al. 2023) is designed for evaluating image-context reasoning, comprising 346 images paired with 1,129 questions crafted by human experts. HallusionBench takes into account both language hallucinations and visual illusions across a diverse range of topics. 5) MMMU (Yue et al. 2023) collects 11.5K multimodal questions from college exams, quizzes, and textbooks, covering six core disciplines, spanning 30 subjects and 183 subfields, including 30 heterogeneous image types. 6) CCBench (Liu et al. 2023c), developed by the MMBench team, is specifically

designed to evaluate MLLMs in the domain of Chinese Culture. 7) SeedBench (Li et al. 2023) encompasses 19K multiple choice questions, covering 12 evaluation dimensions, including both image and video. We only use questions with images for evaluation. 8) BLINK (Fu et al. 2024) contains 14 visual perception tasks which pose significant challenges for current multimodal LLMs.

**Fine-grained Benchmarks.** 1) AI2D (Kembhavi et al. 2016) emphasizes diagram interpretation and reasoning, comprising 5,000 diagrams and 15,000 questions and answers. 2) OCRBench (Liu et al. 2023d) aims to facilitate the assessment of MLLM OCR capabilities, including 29 datasets. 3) TextVQA (Singh et al. 2019) consists of 45,336 questions and 28,408 images that necessitate reasoning about text for answering. We use the validation set, containing 5,000 images, for evaluation. 4) ChartQA (Masry et al. 2022) is a large-scale benchmark featuring 20,882 charts, with questions focusing on logical and visual reasoning. 5) DocVQA (Mathew, Karatzas, and Jawahar 2021) concentrates on document image understanding, encompassing 50,000 questions and over 12,000 images. We evaluate using the validation set, which includes 5,349 questions and 1,286 images. 6) Seed2 Plus (Li et al. 2024a) specifically designed for text-rich visual comprehension evaluation of MLLMs, includes 2.3K multiple-choice questions covering charts, maps, and webs.

## Comparisons with State-of-the-art Models

**General Benchmarks.** In Tab. 2, we compare EE-MLLM with various state-of-the-art MLLMs (Liu et al. 2024; Bai et al. 2023; Ma et al. 2024), across eight general benchmarks. These benchmarks evaluate the comprehensive ability of MLLMs, including understanding and perception, as well as the severity of illusion. These factors collectively reflect the generalization ability and applicability of MLLMs in real-world scenarios. EE-MLLM achieves comparable performance with state-of-the-art MLLMs in general benchmarks. Specifically, EE-MLLM achieves a score of 70.4 in MMBench and 1528.1 in MME, scores that are notably higher compared to LLaVA-v1.6, which also support high-

Model	LLM	AI2D	OCRBench	TextVQA	ChartQA	DocVQA	Seed2 Plus
InstructBLIP	Vicuna-7B	40.6	27.6	33.6	10.9	-	29.5
MiniGPT-4-v1	Vicuna-7B	28.4	17.2	-	-	-	15.2
MiniGPT-4-v2	Llama2-7B	30.5	3.1	-	-	-	23.3
Idefics-instruct	Llama-7B	42.2	25.2	-	-	-	35.4
OpenFlamingo v2	MPT-7B	31.7	14.9	16.3	-	-	28.7
Qwen-VL	Qwen-7B	57.7	12.7	63.1	59.0	-	40.1
Qwen-VL-Chat	Qwen-7B	63.0	48.8	60.7	49.8	-	40.6
ShareGPT4V	Vicuna-7B	58.0	37.1	51.1	21.3	-	46.1
LLaVA-v1.5	Vicuna-7B	55.5	31.8	45.5	17.8	-	41.3
LLaVA-v1.6	Vicuna-7B	67.0	53.2	64.4	55.4	-	51.6
EE-MLLM	Vicuna-7B	65.7	57.4	69.0	68.4	67.4	53.5

Table 3: Comparison with state-of-the-art methods on fine-grained benchmarks, including AI2D, OCRBench, TextVQA, ChartQA, DocVQA, InfoVQA, and SeedBench-2 Plus.

Model	MMB-VAL	SeedBench	ScienceQA	BLINK	AI2D	OCRBench	TextVQA	ChartQA	Avg.
$336 \times 336$									
LLaVA-v1.5	67.3	65.1	67.0	40.7	56.4	24.4	46.1	17.9	48.1
EE-MLLM	66.8	64.1	66.7	38.4	56.2	23.6	43.3	17.3	47.1
$672 \times 672$									
LLaVA-v1.5	70.1	68.0	69.4	40.1	58.3	39.8	61.7	27.9	54.4
EE-MLLM	68.2	67.3	69.1	40.3	57.5	37.0	60.1	25.1	53.1

Table 4: Comparisons with LLaVA under the same settings, including LLM, vision encoder and training data.

resolution images input. This suggests that EE-MLLM possesses comprehensive perception and reasoning capabilities. What’s more, EE-MLLM also achieves promising performance on CCBench and SeedBench.

**Fine-grained Benchmarks.** In Tab. 3, we perform evaluations on seven fine-grained benchmarks. These benchmarks necessitate impressive visual perception capability of MLLMs, as they require the exploration of fine-grained information within images to answer the questions. For traditional VQA benchmarks, such as TextVQA, ChartQA, and DocVQA, MLLM achieves a very impressive performance, 4.6 higher on TextVQA and 13.0 higher on ChartQA compared to LLaVA-v1.6, which also supports high resolution. In the OCRBench, specifically designed to assess the OCR capabilities of MLLM, EE-MLLM outperforms by 4.2 compared to LLaVA-v1.6. These results demonstrate that despite EE-MLLM significantly reducing the computational overhead associated with visual tokens, it effectively maintains the model’s fine-grained capabilities.

### Comparisons of Inference Speed

Despite the significant reduction in FLOPs demonstrated by EE-MLLM, it is crucial to consider real-world scenarios where advanced techniques such as KVCache and Batch Inference are typically employed during deployment. Hence, conducting comparisons of inference speed with these techniques becomes necessary. We conduct the comparisons of inference speed on a single NVIDIA H800. The resolution of the input image is set to  $980 \times 980$ , and the number of generated tokens varies from 2 to 256. We illustrate the speed ratio between EE-MLLM and LLaVA in Fig. 4. Our findings

show that when generating 8 tokens, EE-MLLM’s inference speed is three times that of LLaVA. However, as the number of generated tokens increases, the speed ratio decreases. When generating 64 tokens, EE-MLLM’s inference speed is 1.6 times that of LLaVA. The reason for this observation is that our EE-MLLM primarily reduces the computational cost during the prefilling stage, which calculates the KV cache of visual tokens. The generation of the first token is faster than self-attention-based methods like LLaVA. However, the advantage in inference speed diminishes after the first token. Specifically, with two input images, the inference speed of EE-MLLM is nearly four times that of LLaVA. This clearly indicates that EE-MLLM is significantly more efficient in multi-image input scenarios, including interleaved image-text dialogues and multimodal in-context learning.

Stage	EE-MLLM	LLaVA
Pre-training	32G	75G
Fine-tuning	66G	69G

Table 5: Memory usage of GPU during pre-training and fine-tuning stages.

### GPU Memory Overhead of EE-MLLM

We assess the GPU memory overhead of EE-MLLM during both the pre-training and fine-tuning stages. Similarly, we compare EE-MLLM with LLaVA at a resolution of  $336 \times 336$ . We perform experiments on  $8 \times H800$ , with a global batch size of 256 for pre-training, 128 for fine-tuning.



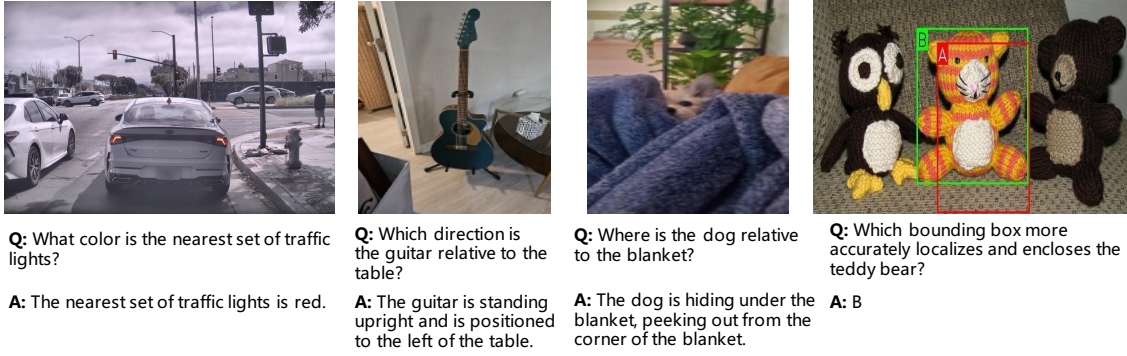


Figure 3: The visualization results of examples sampled from BLINK and RealWorldQA.

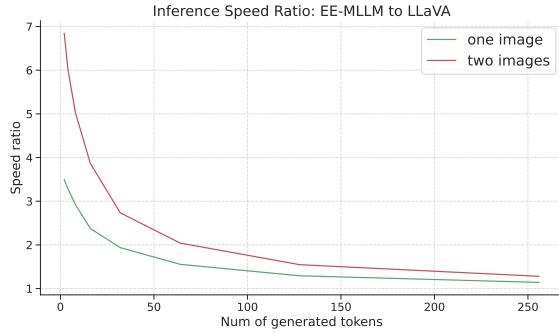


Figure 4: Illustration of Inference Speed Ratio between EE-MLLM and LLaVA for input resolutions of  $980 \times 980$ , considering numbers of generated tokens ranging from 2 to 256, for single and double image inputs.

The comparison of memory usage is detailed in Tab 5. During the pre-training stage, EE-MLLM exhibits significant lower memory usage, at 32G, while the memory usage of LLaVA is 75G. During the fine-tuning stage, as the primary memory usage is focused on the trainable LLM, the memory usage advantage becomes less noticeable, with EE-MLLM consuming 66G and LLaVA-v1.6 utilizing 69G.

## Ablation Study

### Implementation Details

Following LLaVA-v1.5 (Liu et al. 2023a), we employ Vicuna-7b-v1.5 (Zheng et al. 2023) as our foundational LLM. The training data is consistent with LLaVA-v1.5, encompassing both pre-training data and supervised fine-tuning data.

### Comparisons with LLaVA

In Tab. 4, we compare EE-MLLM with LLaVA under the same settings across both general and fine-grained benchmarks. For the resolution of  $336 \times 336$ , we employ CLIP-ViT-L-14 as the vision encoder, ensuring complete alignment with LLaVA-v1.5. EE-MLLM demonstrates comparable performance to LLaVA on general benchmarks. In

V	O	FFN	SeedB	Hall	TextVQA	ChartQA	DocVQA	Avg.
<b><math>336 \times 336</math></b>								
			65.3	24.4	44.8	14.4	18.4	33.5
	✓	✓	66.3	25.9	45.5	16.7	19.2	34.7
✓		✓	65.4	25.3	45.4	15.6	19.1	34.2
✓	✓		65.8	25.1	43.5	14.8	17.9	33.4
✓	✓	✓	66.1	25.7	46.1	15.8	18.6	34.5
<b><math>672 \times 672</math></b>								
			66.1	25.2	56.8	19.7	28.6	39.3
	✓	✓	66.6	25.5	58.2	23.0	29.8	40.6
✓		✓	66.1	24.3	58.2	21.6	30.1	40.1
✓	✓		66.4	24.1	56.3	18.5	26.5	38.4
✓	✓	✓	66.9	27.6	58.8	24.0	31.8	41.8

Table 6: Ablation of the aligner. Checkmarks indicate the weights employed in the aligner.

terms of fine-grained benchmarks, at  $336 \times 336$  resolution, EE-MLLM exhibits promising performance on AI2D and ChartQA but slightly underperforms LLaVA on OCRBench and TextVQA. The average score for the  $336 \times 336$  resolution is 47.1, which is 98% of LLaVA’s 48.1. For the resolution of  $672 \times 672$ , we utilize SigLIP as the vision encoder. As shown in Tab. 4, EE-MLLM obtains comparable results on AI2D and TextVQA, and the average score maintains 98% of LLaVA’s performance.

### Ablation of the Aligner

In Tab. 6, we evaluate the aligner variants with different mapping weights. We employ SigLIP initialized from Idefics2 (Laurençon et al. 2024) to conduct experiments at different input resolutions. We remove the different weights from the aligner and train the model at a resolution of  $336 \times 336$ . Checkmarks indicate the weights employed in the aligner. We have three findings: 1) Removing the entire aligner, as depicted in the first row, significantly reduces performance across multiple benchmarks. Specifically, the TextVQA score drops from 46.1 to 44.8, and the average score for the five benchmarks decreases from 34.5 to 33.5. This result highlights the aligner’s effectiveness in aligning visual features with the LLM feature space, allowing text tokens to capture crucial visual information and address questions through causal cross-attention modules. 2) When ablating individual weights in the aligner, we find that maintaining the structure is more critical. The absence of

$V$  or  $O$  has a relatively minor impact on low-resolution input, even resulting in slightly higher average performance when  $V$  is missing. However, when the FFN is missing, the aligner’s structure no longer resembles a transformer block, leading to a significant performance loss. 3) We directly increase the input image resolution to  $672 \times 672$  without additional training and compare the variants with different aligner types. We observe that, at high-resolution input, the absence of  $V$  or  $O$  weights results in a substantial decline in fine-grained benchmarks such as TextVQA, ChartQA, and DocVQA. This finding demonstrates the importance of a complete aligner when applied to high-resolution images.

## Visualization

We present four examples sampled from BLINK (Fu et al. 2024) and RealWorldQA (XAI 2024) to assess the impact of the architectural changes in Fig 3. The first example demonstrates that EE-MLLM can perceive fine-grained visual context within the image, such as the color of traffic lights. The second and third examples highlight EE-MLLM’s ability to comprehend the position of objects. Specifically, EE-MLLM can accurately identify guitar’s position relative to the table and the dog’s position. The last example reveals that EE-MLLM can distinguish subtle differences in visual content.

## Conclusion

In this paper, we revisit previous studies on multimodal large language models and categorize them into two groups: self-attention-based methods and cross-attention-based methods. The former is data-efficient but computationally inefficient, while the latter is compute-efficient but data-inefficient. To ensure data-efficient while maintaining compute-efficient, we propose the composite attention mechanism for EE-MLLM, which incorporates the composite attention module for computational efficiency and the aligner for data efficiency. We conduct comprehensive experiments on general benchmarks and fine-grained benchmarks and find that EE-MLLM achieves state-of-the-art performance on most benchmarks. We also assess the inference speed of EE-MLLM in real-world scenarios, and the results demonstrate that EE-MLLM holds a significant advantage in inference.

## References

Alayrac, J.-B.; Donahue, J.; Luc, P.; Miech, A.; Barr, I.; Hasson, Y.; Lenc, K.; Mensch, A.; Millican, K.; Reynolds, M.; et al. 2022. Flamingo: a visual language model for few-shot learning. *Advances in neural information processing systems*, 35: 23716–23736.

Awadalla, A.; Gao, I.; Gardner, J.; Hessel, J.; Hanafy, Y.; Zhu, W.; Marathe, K.; Bitton, Y.; Gadre, S.; Sagawa, S.; et al. 2023. Openflamingo: An open-source framework for training large autoregressive vision-language models. *arXiv preprint arXiv:2308.01390*.

Bai, J.; Bai, S.; Yang, S.; Wang, S.; Tan, S.; Wang, P.; Lin, J.; Zhou, C.; and Zhou, J. 2023. Qwen-vl: A frontier large vision-language model with versatile abilities. *arXiv preprint arXiv:2308.12966*.

Carter, J. 2024. TextOCR-GPT4V. <https://huggingface.co/datasets/jimmycarter/textocr-gpt4v>.

Cha, J.; Kang, W.; Mun, J.; and Roh, B. 2024. Honeybee: Locality-enhanced projector for multimodal llm. In *Proceedings of the IEEE/CVF Conference on Computer Vision and Pattern Recognition*, 13817–13827.

Chen, J.; Zhu, D.; Shen, X.; Li, X.; Liu, Z.; Zhang, P.; Krishnamoorthi, R.; Chandra, V.; Xiong, Y.; and Elhoseiny, M. 2023a. MiniGPT-v2: large language model as a unified interface for vision-language multi-task learning. *arXiv preprint arXiv:2310.09478*.

Chen, K.; Shen, D.; Zhong, H.; Zhong, H.; Xia, K.; Xu, D.; Yuan, W.; Hu, Y.; Wen, B.; Zhang, T.; et al. 2024. EVLM: An Efficient Vision-Language Model for Visual Understanding. *arXiv preprint arXiv:2407.14177*.

Chen, L.; Li, J.; Dong, X.; Zhang, P.; He, C.; Wang, J.; Zhao, F.; and Lin, D. 2023b. Sharegpt4v: Improving large multi-modal models with better captions. *arXiv preprint arXiv:2311.12793*.

Dai, W.; Li, J.; Li, D.; Tiong, A. M. H.; Zhao, J.; Wang, W.; Li, B.; Fung, P. N.; and Hoi, S. 2024. Instructblip: Towards general-purpose vision-language models with instruction tuning. *Advances in Neural Information Processing Systems*, 36.

Duan, H.; Yang, J.; Qiao, Y.; Fang, X.; Chen, L.; Liu, Y.; Dong, X.; Zang, Y.; Zhang, P.; Wang, J.; Lin, D.; and Chen, K. 2024. VLMEvalKit: An Open-Source Toolkit for Evaluating Large Multi-Modality Models. *arXiv:2407.11691*.

Fang, R.; Yan, S.; Huang, Z.; Zhou, J.; Tian, H.; Dai, J.; and Li, H. 2023. InstructSeq: Unifying Vision Tasks with Instruction-conditioned Multi-modal Sequence Generation. *arXiv preprint arXiv:2311.18835*.

Fu, C.; Chen, P.; Shen, Y.; Qin, Y.; Zhang, M.; Lin, X.; Qiu, Z.; Lin, W.; Yang, J.; Zheng, X.; et al. 2023. MME: A Comprehensive Evaluation Benchmark for Multimodal Large Language Models. *arXiv preprint arXiv:2306.13394*.

Fu, X.; Hu, Y.; Li, B.; Feng, Y.; Wang, H.; Lin, X.; Roth, D.; Smith, N. A.; Ma, W.-C.; and Krishna, R. 2024. Blink: Multimodal large language models can see but not perceive. *arXiv preprint arXiv:2404.12390*.

Guan, T.; Liu, F.; Wu, X.; Xian, R.; Li, Z.; Liu, X.; Wang, X.; Chen, L.; Huang, F.; Yacoob, Y.; Manocha, D.; and Zhou, T. 2023. HallusionBench: An Advanced Diagnostic Suite for Entangled Language Hallucination & Visual Illusion in Large Vision-Language Models. *arXiv:2310.14566*.

Jia, C.; Yang, Y.; Xia, Y.; Chen, Y.-T.; Parekh, Z.; Pham, H.; Le, Q.; Sung, Y.-H.; Li, Z.; and Duerig, T. 2021. Scaling up visual and vision-language representation learning with noisy text supervision. In *International conference on machine learning*, 4904–4916. PMLR.

Johnson, J.; Hariharan, B.; Van Der Maaten, L.; Fei-Fei, L.; Lawrence Zitnick, C.; and Girshick, R. 2017. Clevr: A diagnostic dataset for compositional language and elementary visual reasoning. In *Proceedings of the IEEE conference on computer vision and pattern recognition*, 2901–2910.



- Kafle, K.; Price, B.; Cohen, S.; and Kanan, C. 2018. Dvqa: Understanding data visualizations via question answering. In *Proceedings of the IEEE conference on computer vision and pattern recognition*, 5648–5656.
- Kembhavi, A.; Salvato, M.; Kolve, E.; Seo, M.; Hajishirzi, H.; and Farhadi, A. 2016. A diagram is worth a dozen images. In *Computer Vision–ECCV 2016: 14th European Conference, Amsterdam, The Netherlands, October 11–14, 2016, Proceedings, Part IV 14*, 235–251. Springer.
- Kirillov, A.; Mintun, E.; Ravi, N.; Mao, H.; Rolland, C.; Gustafson, L.; Xiao, T.; Whitehead, S.; Berg, A. C.; Lo, W.-Y.; et al. 2023. Segment anything. In *Proceedings of the IEEE/CVF International Conference on Computer Vision*, 4015–4026.
- LAION. 2023. GPT-4V Dataset. <https://huggingface.co/datasets/laion/gpt4v-dataset>.
- Laurençon, H.; Tronchon, L.; Cord, M.; and Sanh, V. 2024. What matters when building vision-language models? *arXiv preprint arXiv:2405.02246*.
- Laurençon, H.; Saulnier, L.; Tronchon, L.; Bekman, S.; Singh, A.; Lozhkov, A.; Wang, T.; Karamcheti, S.; Rush, A. M.; Kiela, D.; Cord, M.; and Sanh, V. 2023. OBELICS: An Open Web-Scale Filtered Dataset of Interleaved Image-Text Documents. *arXiv:2306.16527*.
- Li, B.; Ge, Y.; Chen, Y.; Ge, Y.; Zhang, R.; and Shan, Y. 2024a. Seed-bench-2-plus: Benchmarking multimodal large language models with text-rich visual comprehension. *arXiv preprint arXiv:2404.16790*.
- Li, B.; Wang, R.; Wang, G.; Ge, Y.; Ge, Y.; and Shan, Y. 2023. Seed-bench: Benchmarking multimodal llms with generative comprehension. *arXiv preprint arXiv:2307.16125*.
- Li, J.; Li, D.; Xiong, C.; and Hoi, S. 2022. Blip: Bootstrapping language-image pre-training for unified vision-language understanding and generation. In *International conference on machine learning*, 12888–12900. PMLR.
- Li, Z.; Yang, B.; Liu, Q.; Ma, Z.; Zhang, S.; Yang, J.; Sun, Y.; Liu, Y.; and Bai, X. 2024b. Monkey: Image Resolution and Text Label Are Important Things for Large Multi-modal Models. In *proceedings of the IEEE/CVF conference on computer vision and pattern recognition*.
- Lin, Z.; Liu, C.; Zhang, R.; Gao, P.; Qiu, L.; Xiao, H.; Qiu, H.; Lin, C.; Shao, W.; Chen, K.; et al. 2023. Sphinx: The joint mixing of weights, tasks, and visual embeddings for multi-modal large language models. *arXiv preprint arXiv:2311.07575*.
- Liu, H.; Li, C.; Li, Y.; and Lee, Y. J. 2023a. Improved baselines with visual instruction tuning. *arXiv preprint arXiv:2310.03744*.
- Liu, H.; Li, C.; Li, Y.; Li, B.; Zhang, Y.; Shen, S.; and Lee, Y. J. 2024. LLaVA-NeXT: Improved reasoning, OCR, and world knowledge.
- Liu, H.; Li, C.; Wu, Q.; and Lee, Y. J. 2023b. Visual Instruction Tuning. In *NeurIPS*.
- Liu, Y.; Duan, H.; Zhang, Y.; Li, B.; Zhnag, S.; Zhao, W.; Yuan, Y.; Wang, J.; He, C.; Liu, Z.; Chen, K.; and Lin, D. 2023c. MMBench: Is Your Multi-modal Model an All-around Player? *arXiv:2307.06281*.
- Liu, Y.; Li, Z.; Yang, B.; Li, C.; Yin, X.; Liu, C.-l.; Jin, L.; and Bai, X. 2023d. On the hidden mystery of ocr in large multimodal models. *arXiv preprint arXiv:2305.07895*.
- Loshchilov, I.; and Hutter, F. 2018. Decoupled Weight Decay Regularization. In *International Conference on Learning Representations*.
- Lu, H.; Liu, W.; Zhang, B.; Wang, B.; Dong, K.; Liu, B.; Sun, J.; Ren, T.; Li, Z.; Sun, Y.; et al. 2024. DeepSeek-VL: towards real-world vision-language understanding. *arXiv preprint arXiv:2403.05525*.
- Lu, P.; Mishra, S.; Xia, T.; Qiu, L.; Chang, K.-W.; Zhu, S.-C.; Taffjord, O.; Clark, P.; and Kalyan, A. 2022. Learn to Explain: Multimodal Reasoning via Thought Chains for Science Question Answering. In *The 36th Conference on Neural Information Processing Systems (NeurIPS)*.
- Ma, F.; Xue, H.; Wang, G.; Zhou, Y.; Rao, F.; Yan, S.; Zhang, Y.; Wu, S.; Shou, M. Z.; and Sun, X. 2024. Visual Perception by Large Language Model’s Weights. *arXiv preprint arXiv:2405.20339*.
- Masry, A.; Long, D. X.; Tan, J. Q.; Joty, S.; and Hoque, E. 2022. Chartqa: A benchmark for question answering about charts with visual and logical reasoning. *arXiv preprint arXiv:2203.10244*.
- Mathew, M.; Karatzas, D.; and Jawahar, C. 2021. Docvqa: A dataset for vqa on document images. In *Proceedings of the IEEE/CVF winter conference on applications of computer vision*, 2200–2209.
- Methani, N.; Ganguly, P.; Khapra, M. M.; and Kumar, P. 2020. Plotqa: Reasoning over scientific plots. In *Proceedings of the IEEE/CVF Winter Conference on Applications of Computer Vision*, 1527–1536.
- Radford, A.; Kim, J. W.; Hallacy, C.; Ramesh, A.; Goh, G.; Agarwal, S.; Sastry, G.; Askell, A.; Mishkin, P.; Clark, J.; et al. 2021. Learning transferable visual models from natural language supervision. In *ICML*, 8748–8763. PMLR.
- Singh, A.; Natarajan, V.; Shah, M.; Jiang, Y.; Chen, X.; Batra, D.; Parikh, D.; and Rohrbach, M. 2019. Towards vqa models that can read. In *Proceedings of the IEEE/CVF conference on computer vision and pattern recognition*, 8317–8326.
- Wang, J.; Meng, L.; Weng, Z.; He, B.; Wu, Z.; and Jiang, Y.-G. 2023a. To see is to believe: Prompting gpt-4v for better visual instruction tuning. *arXiv preprint arXiv:2311.07574*.
- Wang, L.; Li, L.; Dai, D.; Chen, D.; Zhou, H.; Meng, F.; Zhou, J.; and Sun, X. 2023b. Label words are anchors: An information flow perspective for understanding in-context learning. *arXiv preprint arXiv:2305.14160*.
- XAI. 2024. Grok-1.5V.
- Yao, L.; Li, L.; Ren, S.; Wang, L.; Liu, Y.; Sun, X.; and Hou, L. 2024. DeCo: Decoupling Token Compression from Semantic Abstraction in Multimodal Large Language Models. *arXiv preprint arXiv:2405.20985*.
- Yue, X.; Ni, Y.; Zhang, K.; Zheng, T.; Liu, R.; Zhang, G.; Stevens, S.; Jiang, D.; Ren, W.; Sun, Y.; et al. 2023.

Mmmu: A massive multi-discipline multimodal understanding and reasoning benchmark for expert agi. *arXiv preprint arXiv:2311.16502*.

Zhai, X.; Mustafa, B.; Kolesnikov, A.; and Beyer, L. 2023. Sigmoid loss for language image pre-training. In *Proceedings of the IEEE/CVF International Conference on Computer Vision*, 11975–11986.

Zheng, L.; Chiang, W.-L.; Sheng, Y.; Zhuang, S.; Wu, Z.; Zhuang, Y.; Lin, Z.; Li, Z.; Li, D.; Xing, E. P.; Zhang, H.; Gonzalez, J. E.; and Stoica, I. 2023. Judging LLM-as-a-judge with MT-Bench and Chatbot Arena. *arXiv preprint arXiv:2306.05685*.

Zhu, D.; Chen, J.; Shen, X.; Li, X.; and Elhoseiny, M. 2024. MiniGPT-4: Enhancing Vision-Language Understanding with Advanced Large Language Models. In *ICLR*.